Supporting Information

Brando et al. 10.1073/pnas.0908741107

SI Text

Here we assessed whether the choice of months (July–September) could have influenced the spatial patterns of the enhanced vegetation index (EVI) (West–East and North–South), given the potential for lags in vegetation phenology (e.g., leaf flushing) across the wide ranges of latitude and longitude reported in this study. For instance, one could hypothesize that leaf flushing occurs predominantly in July–October in the East Amazon, in October and November in the Central Amazon, and in November and December in the Western Amazon. These temporal–spatial patterns could create trends of lower EVI from east to west of the Amazon.

Xiao et al. (1) mapped the months with highest EVI [calculated from moderate-resolution imaging spectroradiometer (MODIS) collection 5 reflectances] across the Amazon in 2002 (figure 5b in reference 1). If spatial patterns of EVI were closely associated with gradients in vegetation phenology, the results from (1) are likely to show a consistent shift in the month of highest EVI from West to East and/or South to North of the Amazon. Based on figure 5*b* from that study, we detected no evidence of gradients in vegetation phenology that could explain the strong gradients found in our study.

Because Xiao et al. (1) mapped peak EVI in only 1 y, we repeated their analysis using the Global Inventory Modeling and Mapping Studies (GIMMS) Advanced Very High Resolution Radiometer (AVHRR) Normalized Difference Vegetation Index (NDVI) data set from 1981–2008 (Fig. S6*A*) (2). The GIMMS data generally confirmed the lack of a clear spatial pattern in the timing of peak EVI/NDVI in the Amazon with one exception: There was a potential gradient in the month with highest NDVI from South (earlier in the dry season) to North (later in the dry season/early in the wet season). To make sure that this potential gradient did not influence our conclusions, all statistical models between EVI and climatic variables, for both forest and nonforested areas (Fig. S6*B*), included longitude and latitude as covariates. Although we do not exclude the possibility that the focus on the July–September period may have had some effect on the spatial patterns of EVI, we are confident that the gradients in NBAR-EVI from West to East were not merely an artifact of spatial phenological gradients. Also, the inclusion of latitude and longitude in the statistical models between EVI and climatic variables minimized any potential effect of the choice of month in our conclusions.

1. Xiao X, Hagen S, Zhang Q, Keller M, Moore B (2006) Detecting leaf phenology of seasonally moist tropical forests in South America with multi-temporal MODIS images. *Remote Sensing of Environment* 103:465–473.

2. Tucker CJ, et al. (2005) An extended AVHRR 8-km NDVI dataset compatible with MODIS and SPOT vegetation NDVI data. *Int J Remote Sens* 26:4485–4498.

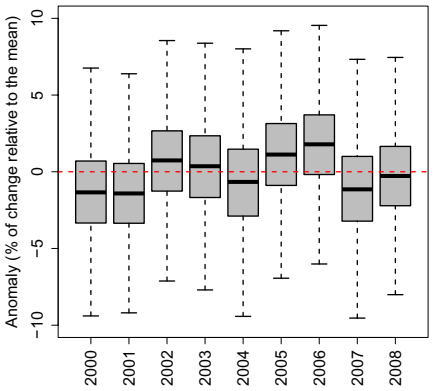

Fig. S1. Boxplots showing EVI anomalies during 2000–2008 across the Amazon. Although outliers (EVIs >95% quantile or <5% quantile) were used to calculate the boxplot statistics, they were not included in the figure to facilitate visualization.

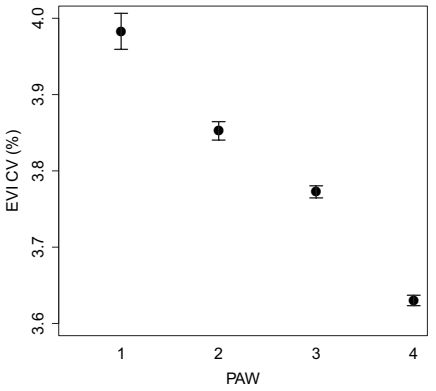

Fig. S2. Average coefficient of variation (CV) of EVI for the entire Amazon, based on data at 500 × 500-m resolution (only for areas with canopy cover ≥70%).

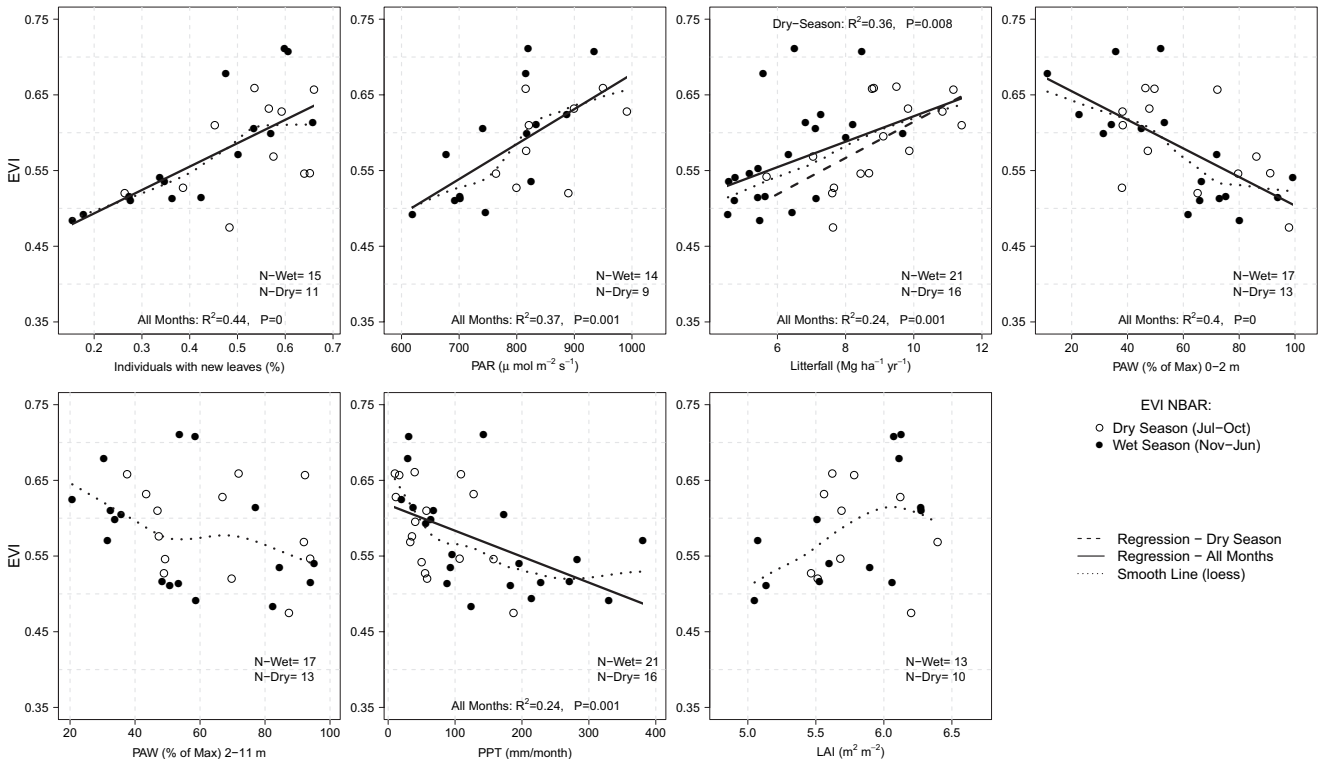

Fig. S3. Site-specific analysis of the relationships between monthly EVI-MODIS Nadir Bidirectional Reflectance Distribution Function (NBAR) and monthly field measurements of individuals with new leaves (%), photosynthetically active radiation (PAR), litterfall, shallow (0–2 m) and deep (2–11 m) plant-available water (PAW), precipitation (PPT), and leaf area index (LAI). The solid and dashed lines represent straight lines fitted using a standard linear regression model for all months and dry season, respectively. The dotted line represents a smooth line.

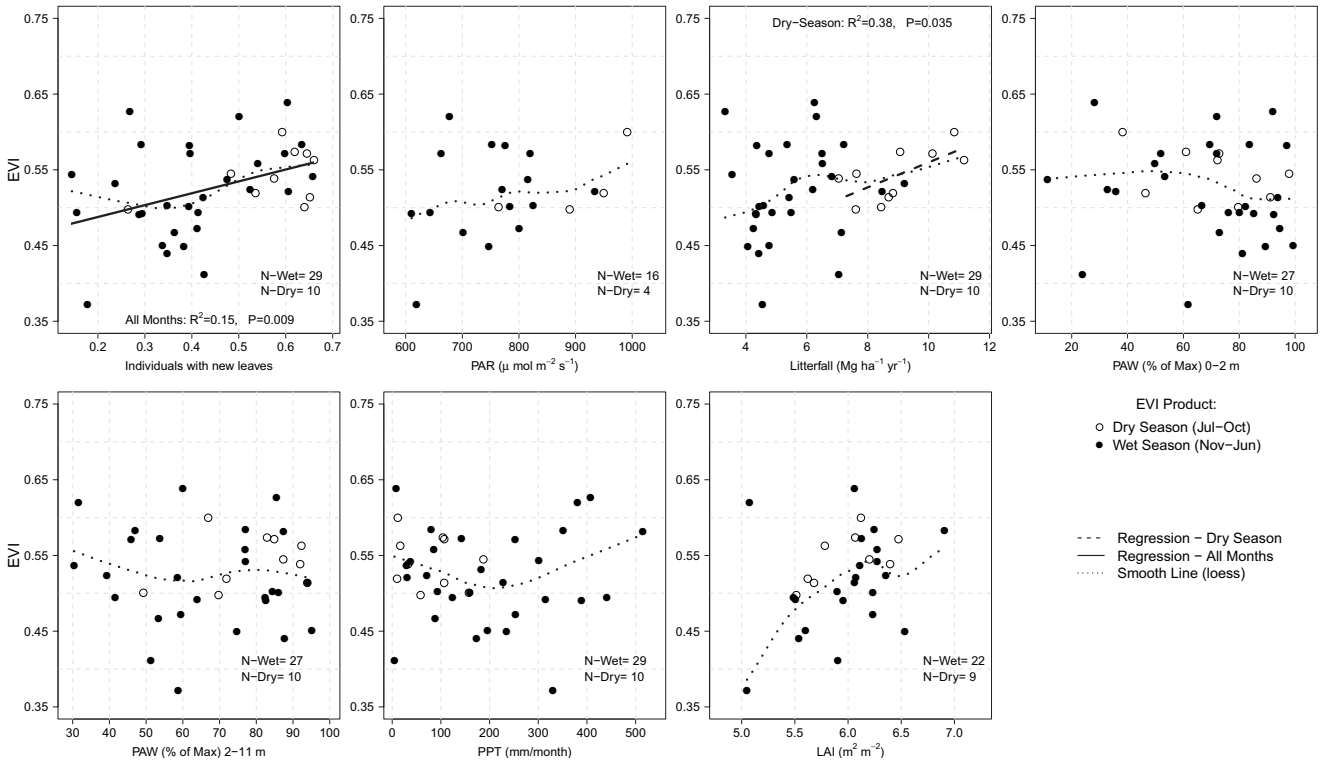

Fig. S4. Site-specific analysis of the relationships between monthly EVI product and monthly field measurements of individuals with new leaves (%), PAR, litterfall, shallow (0–2 m) and deep (2–11 m) PAW, PPT, and LAI. The solid and dashed lines represent straight lines fitted using a standard linear regression model for all months and dry season; respectively. The dotted line represents a smooth line.

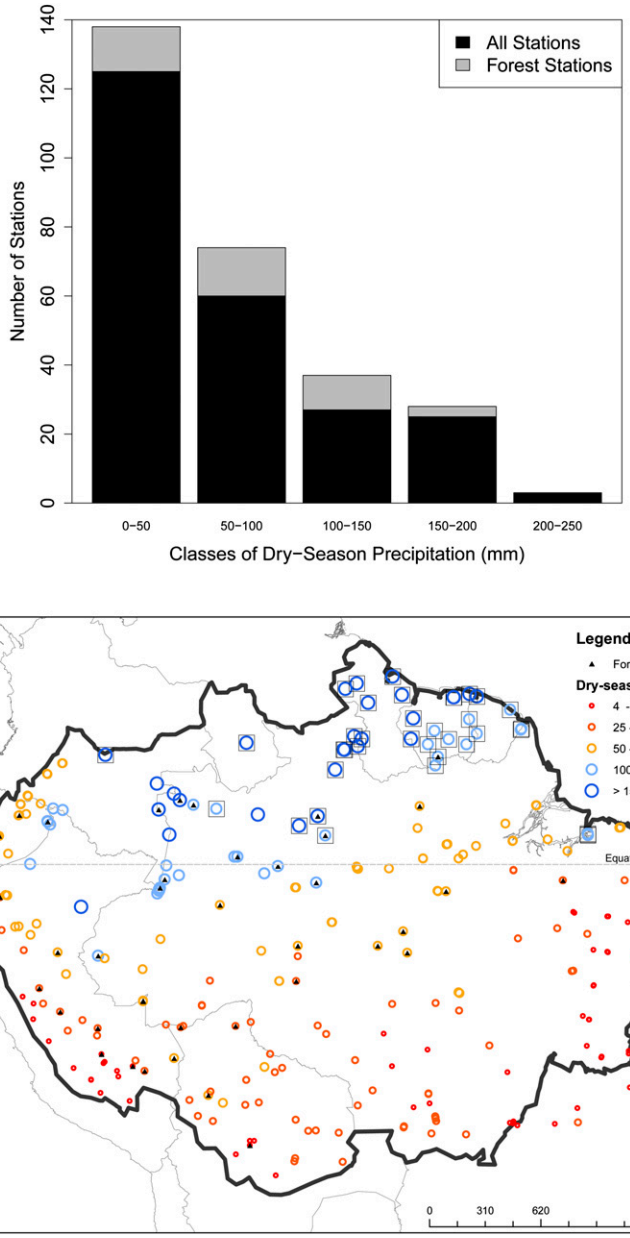

Fig. S5. (*Upper*) The number of meteorological stations per class of precipitation (July–September average). Note that according to the standard definition of dry season as average precipitation <100 mm month^{-1}, the period July–September chosen in this study captured the dry season in 76% of the meteorological stations (212 of 280). For the 68 remaining stations (24%), the average precipitation from July–September was not representative of the driest months of the year in 37 stations (13% of total) concentrated in the Northern Amazon. Note that the total number of meteorological stations in forested areas was 40, that the total number of meteorological stations in forested areas representing the driest months of each year was 37, and that the total number of meteorological stations with dry-season conditions was 27. (*Lower*) Map showing spatial distribution of average dry-season precipitation across the Amazon. Small red circles represent low average dry-season PPT, and large blue circles represent high average dry-season PPT. Black squares represent sites where the months July–September did not capture the driest periods of the year (37 stations; 13% of total). Triangles represent the meteorological stations located in regions with high percentage of canopy cover; 13 meteorological stations were located in regions with no apparent dry season (as defined by <100 mm rain per month), and 37(of 40) meteorological stations were located in regions where July–Sept represented the driest months of the year.

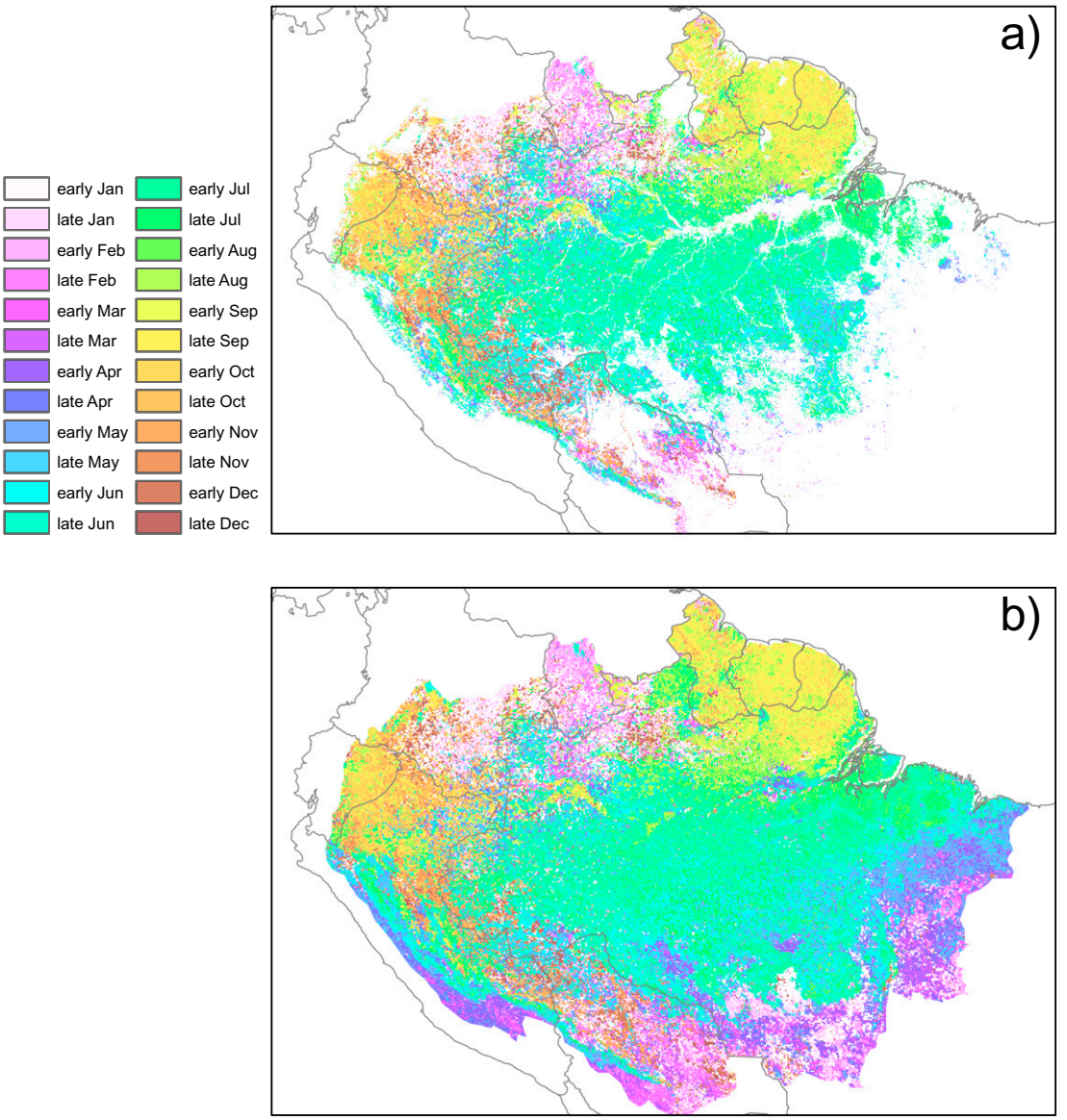

Fig. S6. The month of peak NDVI as recorded in the GIMMS-NDVI dataset between 1981 and 2008 for areas with a high percentage of canopy cover (*A*) and in areas with a wide range of percentage of canopy cover (*B*).

Table S1. ANOVA table for all predictors of EVI in nonforested areas from a linear model (*M1*)

	2000		2001		2002		2003		2004		2005	
Predictor	*F*-value	*P* value	*F*-value	*P* value	*F*-value	*P* value	*F*-value	*P* value	*F*-value	*P* value	*F*-value	*P* value
Intercept	3741.305	<0.0001	4724.746	<0.0001	7069.983	<0.0001	1874.938	<0.0001	8012.448	<0.0001	3165.247	<0.0001
Canopy cover (CC)	66.481	<0.0001	83.257	<0.0001	125.289	<0.0001	96.3497	<0.0001	123.064	<0.0001	138.699	<0.0001
VPD	8.035	0.0057	22.43	<0.0001	31.42	<0.0001	6.7334	0.0108	40.338	<0.0001	9.974	0.0021
PAR	0.882	0.3502	0.028	0.8683	3.771	0.0548	0.9346	0.3359	0.773	0.3813	0	0.9935
PPT	6.834	0.0105	7.06	0.0092	2.656	0.1062	2.2169	0.1395	0.01	0.9211	0.093	0.7604
Longitude	0.949	0.3326	2.056	0.1548	4.301	0.0405	2.0899	0.1512	1.262	0.2637	6.376	0.013
Latitude	3.77	0.0554	1.931	0.1679	10.812	0.0014	7.3007	0.008	19.633	<0.0001	5.551	0.0203
CC*VPD	0.863	0.3555	2.034	0.157	7.889	0.0059	4.0039	0.0479	11.975	0.0008	6.737	0.0108
CC*PAR	0.718	0.3992	0.419	0.5191	0.318	0.5737	4.2554	0.0416	0.046	0.831	0.085	0.7715
CC*PPT	0.196	0.6587	1.57	0.2132	2.898	0.0916	3.0642	0.0829	9.837	0.0022	0.113	0.738

Note that we ran one model for each year of the study.

Table S2. ANOVA table for all predictors of EVI in dense forested areas from a general linear model (*M2*)

Predictor	*F*-value	*P* value
(Intercept)	26359.68	<0.0001
PPT history	2.253	0.1081
PAR	1.111	0.2933
VPD	0.276	0.6
PPT	0.225	0.6359
Latitude	1.826	0.1783
Longitude	5.008	0.0265
PPT history*PAR	0.073	0.93
PPT history*VPD	0.043	0.9577
PPT history*PPT	0.319	0.7274